J Mater Sci: Mater Electron (2013) 24:4270–4278
DOI 10.1007/s10854-013-1396-7

Structural and mechanical characterization of $Bi_{1.75}Pb_{0.25}Sr_2Ca_2Cu_{3-x}Sn_xO_{10+y}$ superconductor ceramics using Vickers microhardness test

H. Koralay · A. Arslan · S. Cavdar · O. Ozturk · E. Asikuzun · A. Gunen · A. T. Tasci

Received: 8 May 2013 / Accepted: 15 July 2013 / Published online: 9 August 2013

Abstract In this work we investigated the role of Sn doping on mechanical and structural properties of $Bi_{1.75}Pb_{0.25}Sr_2Ca_2Cu_{3-x}Sn_xO_{10+y}$ (x = 0.0, 0.1, 0.3 and 0.5) superconducting ceramic material. All samples were fabricated with glass ceramic method. The prepared samples were characterized by using scanning electron microscope (SEM), energy dispersive spectroscopy (EDS), X-ray powder diffractometer (XRD) and static microhardness indenter. Surface morphology, orientation of grains, and elemental composition analysis of the samples were made by SEM and EDS measurements, respectively. Texturing and lattice parameters *a* and *c* were determined by XRD measurements. Load dependent and load independent microhardness, elastic modulus, yield strength and fracture toughness were obtained by hardness measurements. In this work we focused on Vickers microhardness measurements in order to characterize the mechanical properties of our samples. Experimental results of Vickers microhardness measurements were analyzed by using Meyer's law, the elastic/plastic deformation model, proportional sample resistance model (*PSR*), modified PSR model and Hays-Kendall (*HK*) approach. From these analyses, *HK* approach was determined as the most successful model describing the mechanical properties of our samples. Finally in this study, the changes on the mechanical and microstructural properties of Sn doped Bi-2223 superconductors and their possible reasons were also discussed in detail.

H. Koralay · A. Arslan · S. Cavdar · A. Gunen
Superconductivity and Thermal Analysis Laboratory, Department of Physics, Faculty of Sciences, Gazi University, 06531 Ankara, Turkey

O. Ozturk (✉) · E. Asikuzun · A. T. Tasci
Department of Physics, Faculty of Arts and Sciences, Kastamonu University, 37100 Kastamonu, Turkey
e-mail: oozturk@kastamonu.edu.tr

1 Introduction

High temperature superconductors have some basic properties depending on their crystal structure. Most important one is the layered structure they have. Bi–Sr–Ca–Cu–O system is one of the most important high temperature superconductor system that has Cu–O layers in its own structure. $Bi_2Sr_2CaCu_2O_y$ (2212) and $Bi_2Sr_2Ca_2Cu_3O_y$ (2223) structures are widely studied high temperature superconductor structures having Cu–O layers [1–5]. Bi-2212 and Bi-2223 structures have orthorhombic or tetragonal crystal structure. They are also remarkable with their needle-like or flake-like structures.

Producing the crystal structure with different techniques causes some advantages and sometimes disadvantages on the application areas of the obtained superconducting structure. Structures synthesized with glass ceramic method are more homogenous than the structures fabricated with other techniques. However, for the applicability of these structures, some main parameters must be identified initially. For the fabrication of new superconducting material or doping process, determining the mechanical properties of superconductor is as important as its superconducting properties. It is also important to perform appropriate theoretical and experimental studies according to these mechanical properties.

Since it is related with the structure and composition of materials the determination of the hardness of the material is important in analyzing the mechanical properties of superconductors. Hardness can be defined as the measure of resistance of a material against a load applied to its surface. Hardness measurement is commonly preferred to evaluate the quality of materials in industry, because of its nondestructive and easy to perform nature. For ceramic materials, mechanical properties like elastic modulus, yield

strength, fracture toughness and hardness are important as their electrical, magnetic and microstructural properties, since these parameters are crucial for industrial applications of the superconducting materials.

Microhardness of solids depends on the applied load. The phenomenon, known as indentation size effect (ISE); is the decrease of the microhardness value with increase in the applied load [6–8]. ISE behavior depends on many factors like; the load necessary for plastic deformation, elastical recovery, elastic/plastic deformation, the size of the trace resulting from indentation process and the combination of elastic resistance of sample and friction resistance during indentation.

In our study, we calculated the load dependent Vickers microhardness values as well as the load independent microhardness values to analyze the mechanical properties of fabricated samples. Mayer's law, proportional sample resistance model, modified proportional sample resistance model, elastic/plastic deformation model and Hays-Kendall approach were also used to analyze the load independent microhardness values.

2 Experimental procedure

To produce $Bi_{1.75}Pb_{0.25}Sr_2Ca_2Cu_{3-x}Sn_xO_{10+y}$ ($x = 0.0, 0.1, 0.3$ and 0.5) superconducting glass–ceramic sample with appropriate stoichiometric proportions of high purity Bi_2O_3, PbO, $SrCO_3$, $CaCO_3$, SnO_2 and CuO; the powders were mixed in the agate mortar about 1 h. The obtained mixture within alumina crucible was placed into the furnace at room temperature and heated up to 1,150 °C with a step of 10 °C/min heating rate. After, it was kept at this temperature for 1.5 h, the melted mixture was poured between two cooled copper plates to obtain about 0.6-0.8 mm of thick black glasses. These samples were sintered from room temperature to 830 °C with a rate of 10 °C/min, were kept at this temperature for 120 h under oxygen flow.

The lattice parameters of the samples were characterized by using the Bruker D8 Advance X-ray powder diffractometer with Cu–K_α radiation in the range of $5° \leq 2\theta \leq 70^o$ at a scan speed of 2^o/min. The phases in the structure were analyzed with the help of the program Bruker-AXS EVA© 1996–2007 and compared with the international centre for diffraction data card index. Surface morphology and grain orientations of the samples were determined by using Leo EVO-40 VPX scanning electron microscopy (SEM). Moreover, microhardness measurements were also performed on the samples at room temperature via digital microhardness tester Shimadzu HMV-2.

Hereafter, the $Bi_{1.75}Pb_{0.25}Sr_2Ca_2Cu_{3-x}Sn_xO_{10+y}$ superconducting samples produced with $x = 0.0$, 0.1, 0.3 and 0.5 will be expressed as undoped, 0.1, 0.3 and 0.5, respectively.

3 Results and discussion

3.1 XRD analysis

The XRD peaks of the undoped, 0.1, 0.3 and 0.5 samples are shown in the Fig. 1. From this figure one can see that there are peaks belonging to Bi-2212 (041-0317-ICDD), Bi-2223 (042-0743-ICDD) and as an impurity of $SrPbO_3$ (022-1433-ICDD) structures within the pure structure. It is clearly seen that; by the partial substitution of Cu and Sn, the ratio of impurity in the crystal structure increases with Sn ratio (Fig. 1). As can be seen from Fig. 1, the intensities belonging to Bi-2223 phase decreased with increasing doping amount. As is seen, the Sn doped structure $SrSnO_3$ (022-1442-ICDD), Ca_2PbO_4 (003-0131-ICDD) and $Ca_{1.2}Sr_{0.8}PbO_4$ (048-1525-ICDD) impurity peaks occurs and these peaks increase remarkably with the increase in Sn addition. Lattice parameters belonging to high temperature superconductor phases Bi-2212 and Bi-2223 composed by Sn-Cu partial substitution are given in the Table 1. The lattice parameters *a* and *b*, belonging to Bi-2212 phase, remains unchanged while *c* parameter decreases with the Sn addition. However, in Bi-2223 phase, lattice parameters *a* and *b* remains unchanged while *c* parameter increased slightly.

3.2 SEM analysis

Surface structures of Sn doped Bi-2212 and Bi-2223 mixed phase superconductors were analyzed with (SEM). Figure 2 shows the SEM images of undoped and 0.5 samples. As it is seen from this figure, grain sizes increase while the porosity between grains decreases by Sn doping. When undoped and 0.5 samples are compared, 0.5 is seen more intensive and has less porosity than undoped sample. According to these results it is understood that, grain connectivity, orientation and crystallization are improved and formation of needle-like structure became dominant. Increasing the ratio of Bi-2212 phase by doping, supports the needle-like structure characteristic of Bi-2212 superconductors.

3.3 EDS analysis

Atomic component values in Sn doped Bi-2212 samples were analyzed by energy dispersive spectroscopy (EDS) technique. The element concentrations of undoped and 0.5 samples were given in Fig. 3. A decrease in Sr, Cu and Ca ratios was observed by Sn doping. However, the decrease

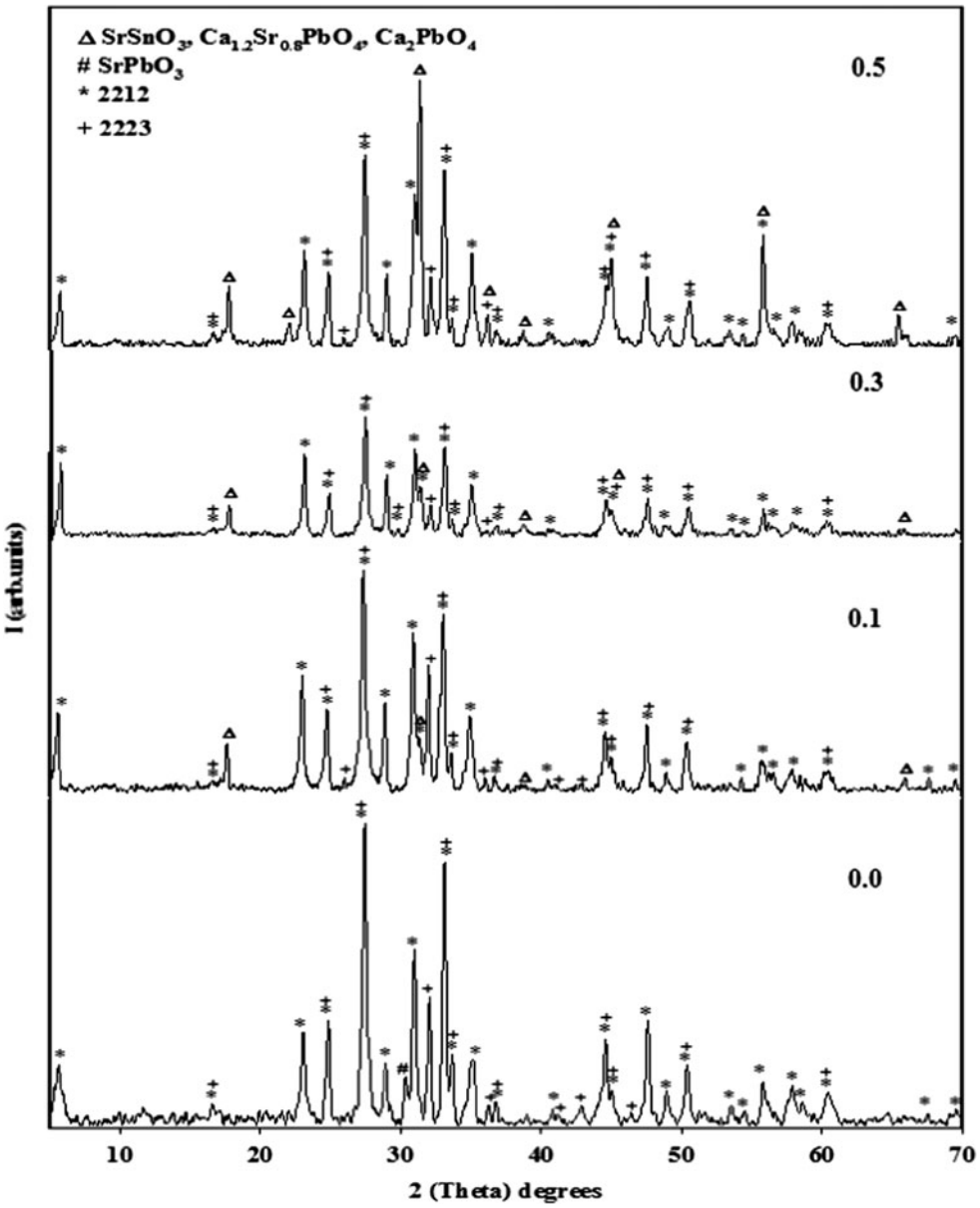

Fig. 1 XRD patterns of the 0.0, 0.1, 0.3 and 0.5 samples

Table 1 Lattice parameter *a, b* and *c* of the all samples

Samples	2212			2223		
	a (Å)	b (Å)	c (Å)	a (Å)	b (Å)	c (Å)
0.0	5.403	5.403	30.806	5.396	5.401	37.212
0.1	5.404	5.404	30.778	5.404	5.399	37.209
0.3	5.404	5.404	30.771	5.399	5.406	37.285
0.5	5.402	5.402	30.721	5.403	5.402	37.240

in Ca groups becomes more dominant. As a result it can be decided that, the Sn +2 ions were entered in the crystal structure are replaced dominantly with Ca +2 ions [9, 10]. In the literature it was reported as, +3 valence rare earth elements were replaced with +2 valence Sr or Ca ions resulting an electron in the structure. This event causes an increase in oxygen content. This oxygen is kept by oxygen deficient Bi–O planes. Eventually, length of the parameter *c* decreases and parameter *a* increases [9]. However this is not case the for our study in which, the *c* parameter is increasing while the *a* parameter stays unchanged by doping in the Bi-2223 system since, Sn atom is +2 valance. The results showed that, the amount of Sn in the sample was increased proportionally with the doping ratio, which indicates the success of doping procedure.

3.4 Vickers microhardness measurements

In this study, the effect of doping on mechanical properties of material was investigated and microhardness values of

undoped and Sn doped $Bi_{1.75}Pb_{0.25}Sr_2Ca_2Cu_{3-x}Sn_xO_{10+y}$ samples prepared by glass ceramic method were also analyzed in detail with some different models. As it is known, hardness is a mechanical parameter and is highly related with composition and structure of solids. Therefore, the importance of microhardness tests is gradually increasing for characterization of a substance [11–16]. There are so many hardness measurement techniques used

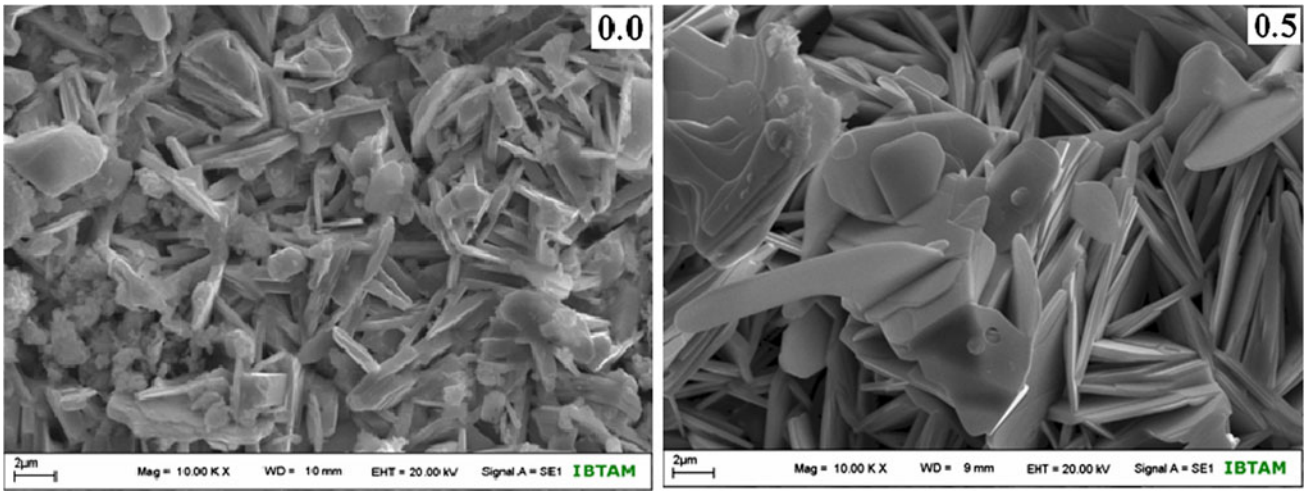

Fig. 2 SEM micrographs of 0.0 and 0.5 samples

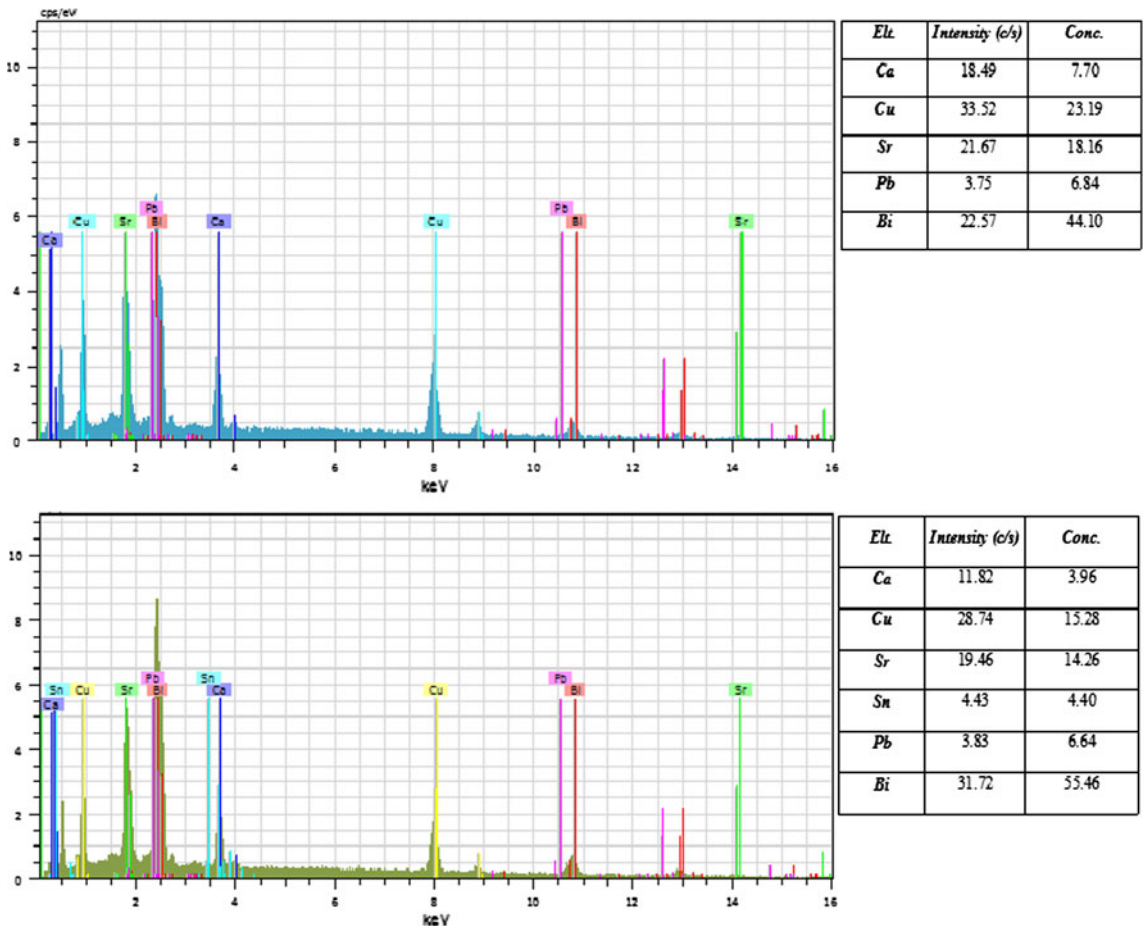

Elt.	Intensity (c/s)	Conc.
Ca	18.49	7.70
Cu	33.52	23.19
Sr	21.67	18.16
Pb	3.75	6.84
Bi	22.57	44.10

Elt.	Intensity (c/s)	Conc.
Ca	11.82	3.96
Cu	28.74	15.28
Sr	19.46	14.26
Sn	4.43	4.40
Pb	3.83	6.64
Bi	31.72	55.46

Fig. 3 Results of EDS measurements of 0.0 and 0.5 samples

today. The basic principles of all these tests are the same. A load is applied on the surface of sample with indenter. After a trace is created on the surface, the indenter is removed. Analysis of microhardness is made by using the diagonal lengths of indentation. Since this test creates a small indentation on the sample surface, it can be easily considered as a non-destructive experiment.

In this study, Vickers microhardness test was used. Vickers microhardness measurements were performed using the digital microhardness device at room temperature in order to determine the doping effect on the mechanical properties of the samples. The applied load, F, was changed within the range of 0.245 N–2.940 N and applied for 10 s. Indenter was suppressed on the different surfaces of the sample. Then Vickers microhardness values (H_v) were calculated using the diagonal length (d) of the indentation as

$$H_v = 1854.4\left(\frac{F}{d^2}\right)(\text{GPa}). \quad (1)$$

In order to obtain a more accurate result, this process was repeated 5 times and the average value of hardness was found. Load dependent microhardness (H_v), elastic modulus (E), yield strength (Y), fracture toughness (K_{IC}) values were also calculated by applying different load for all materials using equations (1–4) as given in Table 2.

Table 2 The calculated load dependent H_v, E, Y, and K_{IC} for the samples

Samples	Load (N)	d (μm)	H_v (GPa)	E (GPa)	Y (GPa)	K_{ic} (Pa/$m^{1/2}$)
0.0	0.245	14.92	2.041	167.29	0.680	1856.39
	0.490	26.64	1.280	104.91	0.426	1470.08
	0.980	39.96	1.138	93.27	0.379	1386.13
	1.960	60.28	0.972	79.66	0.324	1281.01
	2.940	78.13	0.893	73.19	0.297	1227.89
0.1	0.245	17.65	1.458	119.5	0.486	1382.75
	0.490	30.84	0.955	78.27	0.318	1119.07
	0.980	47.30	0.812	66.55	0.270	1031.89
	1.960	71.14	0.718	58.85	0.239	970.36
	2.940	88.37	0.698	57.21	0.232	956.74
0.3	0.245	24.51	0.756	61.96	0.252	833.04
	0.490	46.34	0.423	34.67	0.141	623.14
	0.980	73.76	0.334	27.37	0.111	553.66
	1.960	105.58	0.326	26.72	0.108	547.05
	2.940	130.32	0.321	26.31	0.107	542.84
0.5	0.245	25.75	0.685	56.14	0.228	792.95
	0.490	51.32	0.345	28.27	0.115	562.69
	0.980	75.71	0.317	25.98	0.105	539.42
	1.960	109.16	0.305	24.99	0.101	529.04
	2.940	142.62	0.268	21.96	0.089	495.94

$$E = 81.9635H_v \quad (2)$$

$$Y \approx \frac{H_v}{3} \quad (3)$$

$$K_{IC} = \sqrt{2E\alpha} \quad (4)$$

Here, α is surface energy.

It is apparent from Table 2 that, microhardness values depend on the applied load for undoped and 0.1, 0.3 and 0.5 doped samples. The decrease in the microhardness values, depending on doping rates and applied load are related with impurity phases and irregular grain orientation distribution. As the microhardness value depends on the applied load for the undoped and doped samples, there is a relation between the applied load and indentation size on the sample surface. Smaller indenter load shows higher values of hardness and higher indenter load shows smaller values of microhardness. This observation is associated with the weak grain boundaries of the ceramic metarials. This behavior is called as indentation size effect (*ISE*) in the literature [17, 18].

Figure 4 shows the variations of Vickers microhardness of the samples as a function of the applied load. The decrease in the microhardness values of the samples depending on the increase in doping rates and applied load can also be seen from this figure. The microhardness values reach to plateau limit at about 1 N for all samples.

From Table 2, we can see that for Sn doped samples, the microhardness value decreases with increasing load. It is determined that, the Sn doping does not have any effect on *ISE* behavior, but it is effective on the hardness value of the structure. The elastic modulus (E), yield strength (Y) and fracture toughness (K_{IC}) values decrease significantly with increasing Sn doping. Since these parameters depend on the hardness values; with decreasing the hardness, it is an

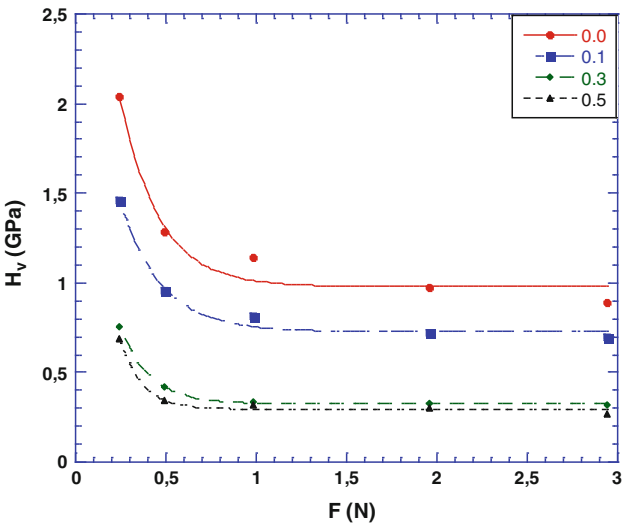

Fig. 4 The variations of microhardness with load for the samples

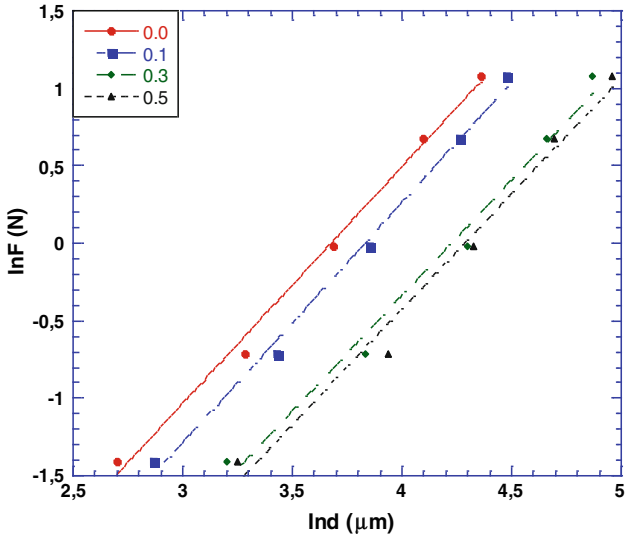

Fig. 5 Variation of applied load *lnF* with diagonal *lnd* for the samples

expected result that, *E*, *Y*, and K_{IC} values decrease. Because, when hardness decrease, elastic modulus, yield strength and fracture toughness decrease accordingly.

The change in microhardness value with applied load reveals the question, "What should be the real hardness value of the sample?" In the literature different models are presented to explain the behavior of the *ISE*. In this section comparisons will be made to calculate the hardness values of our samples using Meyer's Law, Proportional Sample Resistance (*PSR*) Model, Modified Proportional Sample Resistance Model (*MPRS*), Elastic/Plastic Deformation (*EPD*) Model and Hays-Kendall approach (*HK*).

3.4.1 Analysis by Meyer's Law

Meyer's law is the most basic method used in describing the *ISE* behavior. In this method, there is a relationship between the applied load and depth of the trace as

$$F = Ad^{n_K} \tag{5}$$

where, n_K is Meyer number and is obtained from the curves that are fit with the experimental data. n_K is known as Meyer number evaluated as a measure of the behavior of *ISE*. If the n_K value is greater than 2, *RISE* behavior is obtained, and if the n_K value is less than 2, *ISE* behavior is obtained. When n_K is 2, hardness is load independent and this gives the Kick's law to us [11, 12, 19, 20].

Figure 5 shows the variation of applied load In*F* with respect to In*d* for the samples. n_K values was obtained from the slope of the In*F*-In*d* graph are less than 2 for all samples in Fig. 5 and this confirms the *ISE* behavior of load–displacement character for all samples. These data are given in Table 3.

Table 3 Best-fit results of experimental data according to Meyer's law

Samples	n_K	lnA_{1K} (GPa)	H_V (GPa)
0.0	1.52	−5.61	0.893–1.138
0.1	1.55	−5.94	0.698–0.812
0.3	1.49	−6.30	0.321–0.334
0.5	1.48	−6.37	0.268–0.317

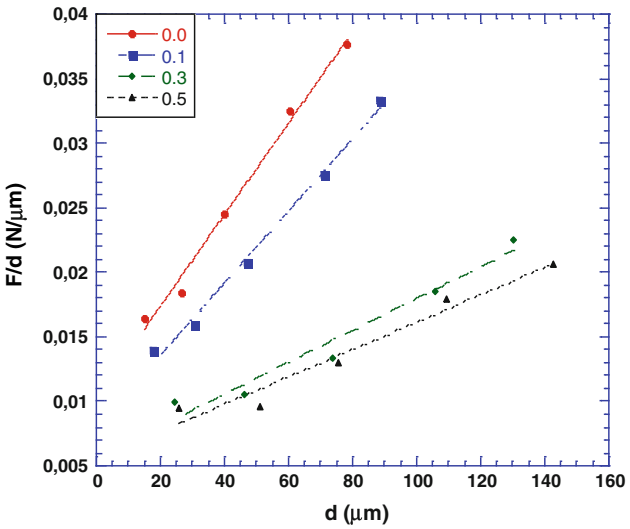

Fig. 6 Plots of *F/d* versus *d* for the samples

Table 4 Best-fit results of experimental data according to *PSR* model

Samples	$\alpha \times 10^{-2}$ (N/μm)	$\beta \times 10^{-3}$ (N/μm^2)	H_{PSR} (GPa)	H_V (GPa)
0.0	1.02	0.35	0.649	0.893–1.138
0.1	0.79	0.27	0.500	0.698–0.812
0.3	0.56	0.12	0.222	0.321–0.334
0.5	0.55	0.10	0.185	0.268–0.317

3.4.2 Analysis by proportional sample resistance model

Proportional sample resistance (*PSR*) model that is used in the microhardness analysis of materials showing *ISE* behavior was developed by Li and Bradt [21]. This model is given with equation (6).

$$F = \alpha d + \beta d^2 \tag{6}$$

$$F/d = \alpha + \beta d \tag{7}$$

where, α is the surface energy and β is a parameter in order to calculate the real hardness value. α and β are calculated from Fig. 6. The change in the value of α is related to the energy dispersion of surface cracks [22]. Load-independent hardness value in *PSR* model is calculated from

$$H_{PRS} = 1854.4\beta \quad (8)$$

In Table 4, values of α, β and H_{PSR} are given. Here, α is positive for all samples confirming that there is also elastic deformation as well as plastic deformation in all samples showing *ISE* behavior. The microhardness values of the samples calculated using *PSR* model [3, 19, 23], given in Table 4, are far from the values of the plateau region obtained from Fig. 4. For this reason the *PSR* model is insufficient on determination of the true hardness values.

In addition, load-independent elastic modulus (E), yield strenght (Y), and fracture toughness (K_{IC}) values were calculated by equations (1–4) using the load independent H_{PSR} values and given in Table 5. By comparing with the load dependent values, it is seen that the load independent E_0, Y_0 and K_{IC} values decrease for doped and undoped samples. The decrease in the value of K_{IC} is related with the reduction of surface energy α. K_{IC} is one of the important mechanical properties of ceramic samples. The selection of materials used for technological applications is an important parameter. Elastic and plastic deformations were observed on the materials obeying *ISE* behavior so, a relaxation occurs on the sample surface after the indenter removed. This situation causes a decrease in the hardness of the material. Toughness also decreases as the microhardness of the sample is decreased. Eventually, we can say that our results are also consistent with the results in the literature [24].

3.4.3 Analysis by modified proportional sample resistance model

According to the *PSR* model, if $d = 0$, the resistance of the test sample $(W = A_1 d)$ is zero [25, 26]. This means the required minimum applied load is zero for a permanent deformation on the material. But, Gong et al. reported that, this definition is not reasonable. Modified proportional sample resistance (*MPSR*) model is given by

$$F = W_{MPSR} + A_{0MPSR}d + A_{1MPSR}d^2 \quad (9)$$

In *MPSR* model, load-independent hardness value can be obtained by using,

$$H_{MPSR} = 1854.4(A_{1MPSR}) \quad (10)$$

Table 5 The calculated load independent H_v, E, Y, and for the samples

Samples	E_0 (GPa)	Y_0 (GPa)	K_{ic} (Pa/m$^{1/2}$)	H_V (GPa)
0.0	53.194	0.216	1041.7	0.893–1.138
0.1	40.982	0.166	804.68	0.698–0.812
0.3	18.196	0.074	451.43	0.321–0.334
0.5	15.163	0.061	408.40	0.268–0.317

In Table 6, A_{MPSR} and W_{MPSR} values were obtained from fitting of the curves in Fig. 7, and associated load-independent hardness values were given. As it can be seen from this table, load-independent hardness values which were calculated according to the *MPSR* model are so far from the results in the plateau region.

3.4.4 Analysis by elastic/plastic deformation model

Dependence of indenter size on the applied load according to Bull et al. [27, 28] is

$$F = A_2(d_p + d_e)^2 \quad (11)$$

Here, A_2 is a constant, d_e is associated with plastic deformation d_p. A_2 and d_e values are calculated from $F^{1/2} - d_p$ graph (Fig. 8). In this model, the load-independent hardness value is calculated by the following equation,

$$H_{EPD} = 1854.4A_2 \quad (12)$$

As it is seen from Table 7, d_e, value which was obtained from slope of the graph, is positive for undoped and Sn doped samples. So, elastic deformation was observed as well as plastic deformation in applied load. As a result elastic recovery was observed for all samples.

3.4.5 Analysis by Hays-Kendall approach

According to Hays-Kendall (*HK*) [29], only elastic deformation was observed under a specific limit value of applied loads and plastic deformation was observed above this limit in the microhardness tests of various materials. This situation was observed by Gane and Bowden [30] as, the indenter cannot penetrate into the sample up to a critical value of applied load. Furthermore, in spite of the applied load increases, indentation size does not increase up to critical value. According to Hays-Kendall, the size of indentation is identified with an effective load $F_{Eff} = F - W_{HK}$ in place of the applied load;

$$F - W_{HK} = A_{HK}d^2 \quad (13)$$

W_{HK} and A_{HK} (a load independent constant) values were calculated from $F - d^2$ graph (Fig. 9). In this model, the load independent hardness value is,

$$H_{HK} = 1854.4A_{HK} \quad (14)$$

W_{HK}, A_{HK} and the load independent microhardness values are given in Table 8. The positive value of W_{HK} can be considered as the applied load is sufficient to create both elastic and plastic deformation [31].

With respect to the other models; the microhardness values, which were obtained from Hays-Kendall approach,

Table 6 Best-fit results of experimental data according to *MPSR* model

Samples	A_{0MPSR}	A_{1MPSR}	W_{MPSR} (N)	H_{MPSR} (GPa)	H_V (plateau region) (GPa)
0.0	0.0128	0.0003	0.0453	0.556	0.893–1.138
0.1	0.0027	0.0003	0.0936	0.556	0.698–0.812
0.3	0.0026	0.0002	0.2066	0.370	0.321–0.334
0.5	0.0048	0.0001	0.0073	0.185	0.268–0.317

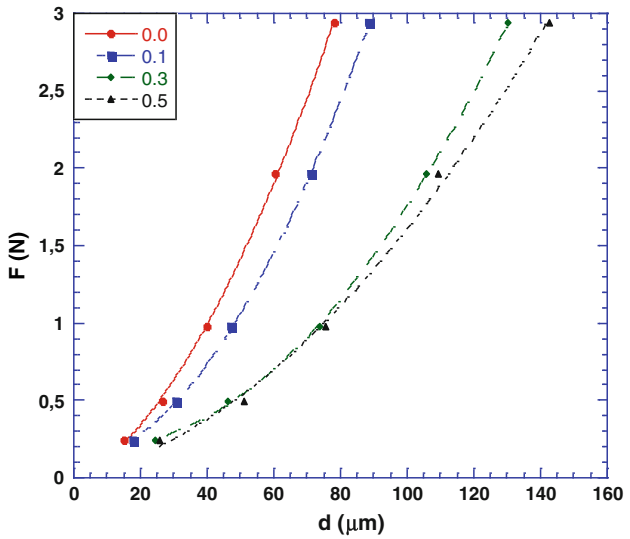

Fig. 7 Plots of F versus d for the samples

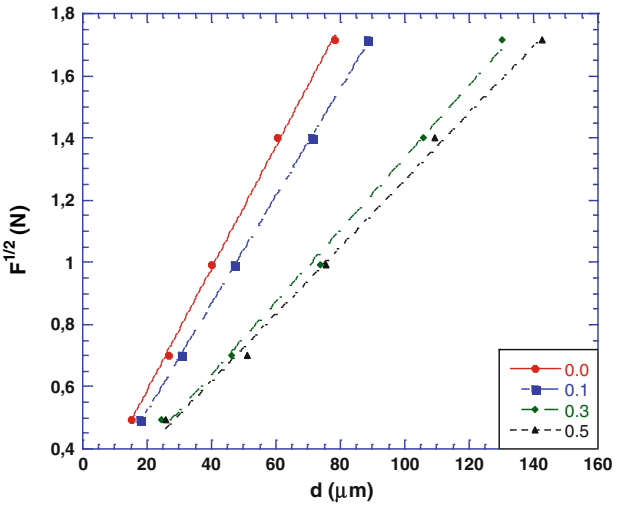

Fig. 8 Plots of diagonal length versus square root of applied loads for the samples

Table 7 Best-fit results of experimental data according to *EPD* model

Samples	A_2 (N/μm^2)	d_e (μm)	H_{EPD} (GPa)	H_V (GPa)
0.0	0.019	0.197	0.669	0.893–1.138
0.1	0.017	0.172	0.535	0.698–0.812
0.3	0.011	0.175	0.224	0.321–0.334
0.5	0.010	0.187	0.185	0.268–0.317

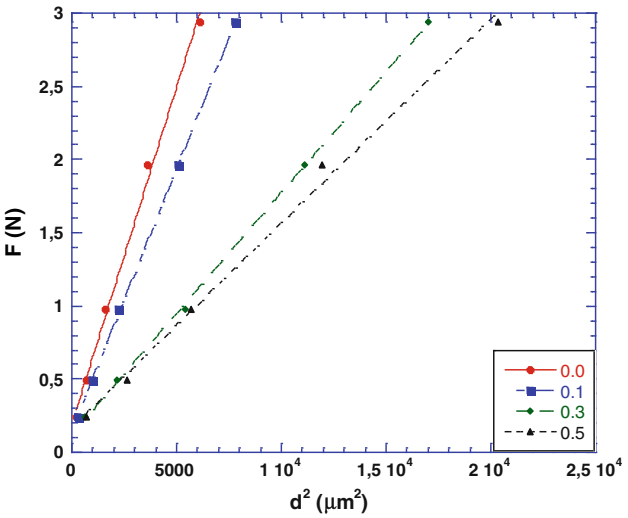

Fig. 9 Applied load versus the square of the impression semi-diagonal length for the samples

Table 8 Best-fit results of experimental data according to *HK* model

Samples	$A_{HK} \times 10^{-5}$	W_{HK} (N)	H_{HK} (GPa)	H_V (Plateau Region) (GPa)
0.0	46.03	0.19	0.853	0.893–1.138
0.1	35.77	0.15	0.663	0.698–0.812
0.3	16.49	0.12	0.305	0.321–0.334
0.5	13.96	0.17	0.258	0.268–0.317

are closer to values at the plateau region for the samples having *ISE* behavior (Table 9). Studies for different materials in the literature [19, 30–33] emphasize that values of the load independent microhardness should be close to the values at the plateau region. For this reason, Hays-Kendall model is the most appropriate one for analyzing the microhardness values and mechanical properties for the samples like ours.

Table 9 The results of load dependent Vickers microhardness at the plateau region and load independent hardness values calculated using *PSR*, *MPSR*, *EPD* and *HK* models

Samples	H_{PSR} (GPa)	H_{MPSR} (GPa)	H_{EDP} (GPa)	H_{HK} (GPa)	H_V (Plateau Region)(GPa)
0.0	0.649	0.556	0.669	0.853	0.893–1.138
0.1	0.500	0.556	0.535	0.663	0.698–0.812
0.3	0.222	0.370	0.224	0.305	0.321–0.334
0.5	0.185	0.185	0.185	0.258	0.268–0.317

4 Conclusions

In this study, the role of Sn doping on the microstructural and mechanical properties of $Bi_{1.75}Pb_{0.25}Sr_2Ca_2Cu_{3-x}Sn_xO_{10+y}$ ceramic superconductors, prepared by glass ceramic method, has been investigated with XRD, SEM, EDS and microhardness measurements. According to the XRD analysis, the lattice parameters *a* and *b* of Bi-2212 phase structure remained unchanged, while the parameter *c* decreased by Sn doping. Similarly, *a* and *b* parameters did not change, but the *c* parameter increased a little for the Bi-2223 phase structure. In addition, XRD results showed that the impurity peaks $SrSnO_3$, Ca_2PbO_4 and $Ca_{1.2}Sr_{0.8}PbO_4$ were composed by partial substitution of Cu-Sn. This result indicates that most Sn atoms enter into the crystal structure of Bi-2212 and Bi-2223 but; they cause the formation of $SrSnO_3$, Ca_2PbO_4 and $Ca_{1.2}Sr_{0.8}PbO_4$ phases out of the structure.

Scanning electron microscope results show that grain size of the samples increase and the surface structure improve by the grain connections. In addition, a significant decrease is observed in the percentage of Ca from the EDS measurements when it's compared with other elements. These results imply that, the Sn atoms doped into Bi-2212 phase, are dominantly replaced with Ca atoms and entered into the crystal structure.

Microhardness measurements performed for the investigation of the effects of Sn atoms on the mechanical properties of materials show us; decrease in hardness via Sn doping. Moreover, *ISE* behavior is also observed for our samples, because microhardness values decrease with applied load. In order to understand this behavior, some models can be used (Meyer's Law, *PSR* model, *MPSR* Model, *EPD* Model and Hays-Kendall approach). The most suitable model describing microhardness of our samples is Hays-Kendall approach.

Acknowledgments The authors thank the financial support for this work through the Scientific Research Projects (BAP 05/2010-61) Foundation of Gazi University Ankara.

References

1. A. Jeremie, K. Alami-Yadri, J.-C. Grivel, R. Flükiger, Supercond. Sci. Technol. **6**, 730–735 (1993)
2. A. Arslan, H. Koralay, Ş. Çavdar, A. Günen, J. Non-Cryst, Solids **358**, 1190–1195 (2012)
3. M. Yilmazlar, O. Ozturk, O. Gorur, I. Belenli, C. Terzioglu, Supercond. Sci. Technol. **20**, 365–371 (2007)
4. H. Koralay, F. Yakuphanoglu, S. Cavdar, A. Gunen, E. Aksu, Phys. B. **355**, 64 (2005)
5. G. Yildirim, M. Dogruer, O. Ozturk, A. Varilci, C. Terzioglu, Y. Zalaoglu, J. Supercond. Nov. Magn. **25**, 893–903 (2012)
6. O. Sahin, O. Uzun, U. Kölemen, B. Duzgun, N. Ucar, Chın. Phys. Lett. **22**(12), 3137 (2005)
7. N.H. Mohammed, A.I. Abou-Aly, I.H. Ibrahim, R. Awad, M. Rekaby, J. Alloy, Compd. **486**, 733–737 (2009)
8. S. Cavdar, E. Deniz, H. Koralay, O. Ozturk, M. Erdem, A. Gunen, J. Supercond. Nov. Magn. **25**, 2297 (2012)
9. O. Ozturk, E. Asikuzun, M. Erdem, G. Yildirim, O. Yildiz, C. Terzioglu, J. Mater Sci, Mater Electron. **23**, 511–519 (2012)
10. A. Biju, P.M. Sarun, R.P. Aloysius, U. Syamaprasad, J. Alloy, Compd. **454**, 46–51 (2008)
11. O. Ozturk, H.A. Cetinkara, E. Asikuzun, M. Akdogan, M. Yilmazlar, C. Terzioglu, J. Mater Sci, Mater Electron. **22**, 1501–1508 (2011)
12. E. Asikuzun, O. Ozturk, H.A. Cetinkara, G. Yildirim, A. Varilci, M. Yılmazlar, C. Terzioglu, J. Mater. Sci.: Mater. Electron. **23**, 1001–1010 (2012)
13. O. Uzun, U. Kölemen, S. Çelebi, N. Güçlü, J. Eur. Ceram. Soc. **25**(6), 969–977 (2005)
14. O. Ozturk, M. Erdem, E. Asikuzun, O. Yildiz, G. Yildirim, A. Varilci, J. Terzioglu, Mater. Sci: Mater Electron. **24**(1), 230–238 (2013)
15. O. Uzun, T. Karaaslan, M. Keskin, J. Alloy, Compd. **358**, 104–111 (2003)
16. Y. Yoshino, A. Iwabuchi, R. Onodera, A. Chiba, K. Katagiri, T. Shimizu, Cryogenics **41**, 505–511 (2001)
17. J. Gong, J. Wu, Z. Guan, J. Eur. Ceram. Soc. **19**, 2625–2631 (1999)
18. A.A. Elmustafa, D.S. Stone, J. Mech. Phys. Solid **51**, 357 (2003)
19. J.B. Quinn, V.D. Quinn, J. Mater. Sci. **32**, 4331–4346 (1997)
20. H.A. Cetinkara, M. Yilmazlar, O. Ozturk, M. Nursoy, C. Terzioglu, J. Phys: Conf. Ser. **153**, 012038 (2009)
21. H. Li, R.C. Bradt, J. Mater. Sci. **28**, 917–926 (1993)
22. A. Leenders, M. Mich, H.C. Freyhard, Physica C **279**, 173 (1997)
23. M. Yilmazlar, H.A. Cetinkara, M. Nursoy, O. Ozturk, C. Terzioglu, Physica C **442**, 101–107 (2006)
24. K. Sangwal, Mater. Chem. Phys. **63**, 145–152 (2000)
25. U. Kölemen, O. Uzun, M. Yılmazlar, N. Güçlü, E. Yanmaz, J. Alloy, Compd. **415**, 300–306 (2006)
26. J. Gong, J. Wu, Z. Guan, Mater. Lett. **38**, 197 (1999)
27. G.P. Upit, S.A. Varchenya, Phys. Status Solidi A **17**, 831 (1966)
28. S.J. Bull, T.F. Page, E.H. Yoffe, Philos. Mag. Lett. **59**, 281 (1989)
29. C. Hays, E.G. Kendall, Metall. **6**, 275–282 (1973)
30. N. Gane, F.P. Bowden, J. Appl. Phys. **39**, 1432–1435 (1968)
31. R. Awad, A.I. Abou-Aly, M. Kamal, M. Anas, J. Supercond. Nov. Magn. **24**, 1947–1956 (2011)
32. L. Arda, O. Ozturk, E. Asikuzun, S. Ataoglu, Powder Technol. **235**, 479–489 (2013)
33. O. Ozturk, E. Asikuzun, G. Yildirim, J. Mater Sci, Mater Electron. **24**, 1271–1274 (2012)